

Feasibility of incorporating phosphogypsum in ettringite-based binder  
from ladle slag

Peer-reviewed author version

GIJBELS, Katrijn; Hoang, Nguyen; Kinnunen, Paivo; SCHROEYERS, Wouter;  
Pontikes, Yiannis; SCHREURS, Sonja & Illikainen, Mirja (2019) Feasibility of  
incorporating phosphogypsum in ettringite-based binder from ladle slag. In:  
JOURNAL OF CLEANER PRODUCTION, 237 (Art N° UNSP 117793).

DOI: 10.1016/j.jclepro.2019.117793

Handle: <http://hdl.handle.net/1942/29722>



Feasibility of incorporating phosphogypsum in ettringite-based binder from ladle slag [Link](#)

**Peer-reviewed author version**

Made available by Hasselt University Library in [Document Server@UHassel](#)

**Reference** (Published version):

Gijbels, Katrijn; Nguyen, Hoang; Kinnunen, Paivo; Schroeyers, Wouter; Pontikes, Yiannis; Schreurs, Sonja & Illikainen, Mirja(2019) Feasibility of incorporating phosphogypsum in ettringite-based binder from ladle slag. In: Journal of cleaner production, 237 (Art N° 117793)

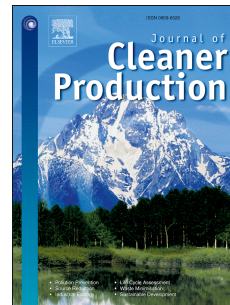
DOI: 10.1016/j.jclepro.2019.117793

Handle: <http://hdl.handle.net/1942/29600>

# Accepted Manuscript

Feasibility Of Incorporating Phosphogypsum In Ettringite-Based Binder From Ladle Slag

Katrijn Gijbels, Hoang Nguyen, Paivo Kinnunen, Wouter Schroeiers, Yiannis Pontikes, Sonja Schreurs, Mirja Illikainen



PII: S0959-6526(19)32653-8

DOI: <https://doi.org/10.1016/j.jclepro.2019.117793>

Article Number: 117793

Reference: JCLP 117793

To appear in: *Journal of Cleaner Production*

Received Date: 30 April 2019

Revised Date: 20 July 2019

Accepted Date: 25 July 2019

Please cite this article as: Katrijn Gijbels, Hoang Nguyen, Paivo Kinnunen, Wouter Schroeiers, Yiannis Pontikes, Sonja Schreurs, Mirja Illikainen, Feasibility Of Incorporating Phosphogypsum In Ettringite-Based Binder From Ladle Slag, *Journal of Cleaner Production* (2019), doi: 10.1016/j.jclepro.2019.117793

This is a PDF file of an unedited manuscript that has been accepted for publication. As a service to our customers we are providing this early version of the manuscript. The manuscript will undergo copyediting, typesetting, and review of the resulting proof before it is published in its final form. Please note that during the production process errors may be discovered which could affect the content, and all legal disclaimers that apply to the journal pertain.

1 **FEASIBILITY OF INCORPORATING PHOSPHOGYPSUM IN**  
2 **ETTRINGITE-BASED BINDER FROM LADLE SLAG**

3

4 Katrijn GIJBELS<sup>a</sup>, Hoang NGUYEN<sup>b\*</sup>, Paivo KINNUNEN<sup>b</sup>, Wouter SCHROEYERS<sup>a</sup>, Yiannis  
5 PONTIKES<sup>c</sup>, Sonja SCHREURS<sup>a</sup>, Mirja ILLIKAINEN<sup>b</sup>

6

7 <sup>a</sup> Hasselt University, CMK, Nuclear Technological Centre, Agoralaan, Gebouw H, 3590  
8 Diepenbeek, Belgium

9 <sup>b</sup> Fibre and Particle Engineering Research Unit, University of Oulu, Pentti Kaiteran katu 1,  
10 90014 Oulu, Finland

11 <sup>c</sup> KU Leuven, Department of Materials Engineering, Kasteelpark Arenberg 44, 3001 Leuven,  
12 Belgium

13 \* Corresponding author: Hoang NGUYEN

14

15 katrijn.gijbels@uhasselt.be, hoang.nguyen@oulu.fi, paivo.kinnunen@oulu.fi,  
16 wouter.schroeyers@uhasselt.be, yiannis.pontikes@kuleuven.be,  
17 sonja.schreurs@uhasselt.be, mirja.illikainen@oulu.fi

18

19 Footnote: The two first authors contributed equally to this research paper.

**Abstract**

Aiming to utilize phosphogypsum (PG) as a construction material, this study investigated the potential use of PG as a calcium sulfate source for the production of an ettringite-based binder (LSG). Six compositions with different percentages and PG's of different origin were hydrated with ladle slag (LS) to form LSG. The hydration, mineralogy and compressive strength of all mixtures were investigated and compared with a reference LSG made of pure synthetic gypsum. The minor impurities in PG, the different particle size distribution as well as the mineralogy induced distinguishable effects on the heat of hydration, phase assemblage and morphology. The results showed that the use of side-stream PG instead of pure gypsum results in superior properties with a 60% increase in compressive strength. This investigation shows high potential to produce a completely by-product-based LSG by combining different sources of industrial side-streams with minimal chemical and energy use.

**Keywords**

Ladle slag; phosphogypsum; ettringite; hydration; mineralogy; compressive strength

**1. Introduction**

Phosphogypsum (PG) is a residue of phosphate production with a very low recycling rate (less than 5%) (International Atomic Energy Agency (IAEA), 2013). Approximately 4 to 6 tonnes of PG are generated for each tonne of phosphoric acid produced (Rashad, 2017). Worldwide, this results in around 170 million tonnes per year of PG being disposed of. The total amount of PG in disposal sites is estimated to reach 7 to 8 billion tonnes by 2025 (International Atomic Energy Agency (IAEA), 2013). In addition, the world population is still increasing and hence food production will continue to grow, which requires an increase in phosphate fertilizer production. Therefore, there will be increasing levels of PG production

45 and disposal, in most cases without purification (Rashad, 2017; Tayibi et al., 2009), which  
46 can cause serious environmental contamination due to impurities. This contamination may  
47 occur from radon gas, atmospheric contamination with fluoride, ground- and groundwater  
48 pollution with naturally occurring radionuclides, acidity, or mobile heavy metal anions  
49 (Cánovas et al., 2018). Therefore, the use of PG in construction materials would take  
50 advantage of the availability of this secondary resource and offer obvious environmental  
51 benefits.

52 Many obstacles hamper the utilization of PG as a construction material, however (Cánovas  
53 et al., 2018; Rashad, 2017), the main one being the presence of certain impurities. For  
54 example, the use of PG can lead to unwanted retarding effects on setting when mixed with  
55 ordinary or blended Portland cement (OPC) (Akin Altun and Sert, 2004; Rashad, 2017;  
56 Saadaoui et al., 2017). The incorporation of PG in OPC also caused a strength reduction  
57 (Smadi et al., 1999). PG may also contain enhanced concentrations of naturally occurring  
58 radionuclides (more specifically, the naturally occurring radium isotopes) (Cánovas et al.,  
59 2018), which limits its use for building applications (e.g. as gypsum board or in cement and  
60 concrete) (Council of the European Union, 2014). Therefore, disposal has remained the  
61 predominant fate for PG. Some studies have suggested pre-treatment of PG such as  
62 calcinating, washing, and mechanical or chemical treatment (Al-Hwaiti, 2015; Hamas-Nasri  
63 et al., 2019; Koopman and Witkamp, 2002; Potgieter et al., 2003; Smadi et al., 1999).  
64 However, the economic feasibility of these treatments is questioned. Consequently, the  
65 possibility to use PG with minor or no treatment is of high interest.

66 An ettringite-based binder, a promising application-dependent alternative to OPC-based  
67 cementitious materials, can be formed by the reaction between Al-rich phases and calcium  
68 sulfate sources. The main crystalline phase of the binder is ettringite ( $C_3A \cdot 3\bar{C}\bar{S} \cdot 32H$ ; refer to  
69 Table 1 for cement notation). The ettringite-based binder is reported to have many  
70 advantages in comparison to OPC: it can attain good mechanical properties (Kim et al.,  
71 2016; Nguyen et al., 2019a), high chemical resistance (Quillin, 2001), and the ability to

72 stabilize heavy metals in its structure (Peysson et al., 2005). In a previous investigation  
73 (Nguyen et al., 2019a, 2019b), an ettringite-based binder (LSG) was produced from the  
74 hydration between ladle slag (LS, a by-product from the steel industry) and pure gypsum.  
75 The microstructure, mechanical properties and durability of the LSG were studied. In  
76 addition, a fiber-reinforced composite from LSG showed high mechanical performance with  
77 very low CO<sub>2</sub> emissions (Nguyen et al., 2019c) compared with other conventional high-  
78 performance OPC-based composites. LS can also react with water without the presence of  
79 calcium sulfate. However, these reaction products are metastable and their conversion leads  
80 to strength reduction at later ages (Nguyen et al., 2019a).

81 To utilize PG in a more efficient way, it is used as a calcium sulfate source in the present  
82 study to produce an ettringite-based binder. Since it consists of mainly CaSO<sub>4</sub>·2H<sub>2</sub>O with  
83 some minor impurities, PG is able to replace pure gypsum partially or completely in the  
84 reaction with LS to form the LSG. The cementitious binder in this work is almost entirely a by-  
85 product-based binder with a minor content of citric acid as a retarder and, hence, is able to  
86 offer both environmental and economic benefits. However, for a better understanding of the  
87 feasibility of reusing PG in LSG, several aspects need to be studied: (1) the effects of  
88 impurities in PG on the fresh and hardened state of LSG; (2) the optimal dosage of PG that  
89 can be used in LSG to obtain good mechanical properties; and (3) the microstructure and  
90 phase characterization of the developed materials.

91 Encouraged by the prospect of better utilization of PG in the construction industry, and to fill  
92 the aforementioned research gaps, this experimental investigation aims to provide an  
93 understanding of the feasibility of using PG as a precursor for LSG. The effects of impurities  
94 from PG on the fresh and hardened state of LSG was studied. The former was investigated  
95 by monitoring the heat of hydration by isothermal calorimetry, while the latter was studied by  
96 assessing the compressive strength up to 3 months of curing. Additionally, the hydration and  
97 the reaction products were monitored using a range of complementary techniques such as X-  
98 ray diffraction (XRD), Fourier-transformed infrared (FTIR) spectroscopy and

99 thermogravimetric analysis (TGA). Morphological analysis was performed with scanning  
100 electron microscopy (SEM). Six compositions with PG's of different origin are the subject of  
101 the present study, and they are compared with the LSG from pure gypsum developed in a  
102 previous study (Nguyen et al., 2019b). In conclusion, the optimized mixture and suggestions  
103 for the use of PG in LSG are proposed and discussed.

104

## 105 **2. Materials and methods**

### 106 **2.1 Materials**

107 The LS was supplied by SSAB Europe Oy (Raahe, Finland). The slag was collected from the  
108 company's slag pit after cooling naturally. The free CaO content was found to be zero,  
109 measured according to EN 450-1 (European Committee for Standardization, 2012). The LS  
110 was ball milled (TPR-D-950-V-FU-EH, Germatec Germany) to reach a  $d_{50}$  value of 10  $\mu\text{m}$ .

111 The density of the LS was measured with a Quantachrome Multipycnometer (MPV-6DC)  
112 according to ASTM C204 (ASTM International, 2017) and was 3.0  $\text{g}/\text{cm}^3$ . The Blaine value of  
113 the LS was determined according to EN 196-6 (European Committee for Standardization,  
114 2010) and was  $2640 \pm 200 \text{ cm}^2/\text{g}$ . As calcium sulfate sources, 3 types of gypsum were used  
115 in this study (hereafter referred to as G1, G2 and G3, respectively). The first type (G1) was  
116 synthetic gypsum ( $\text{CaSO}_4 \cdot 2\text{H}_2\text{O}$ ) supplied by VWR (product code 22451.360). The second  
117 type (G2) was PG derived from Yara Oy (Finland). The third type was a reference material  
118 (n° 434) collected from a PG processing plant in Gdansk (Poland), which was milled and  
119 homogenized by the International Atomic Energy Agency (IAEA) (Shakhashiro et al., 2011).

120 G2 was dried at 60  $^\circ\text{C}$  in a laboratory oven for 24 h to remove all moisture. G1 and G3 were  
121 used as received. The particle size distribution of the LS, G1, G2 and G3 was determined by  
122 laser scattering (Beckman Coulter LS 13 320), using the Fraunhofer model (International  
123 Organization for Standardization (ISO), 2009). Isopropanol was used to avoid hydration  
124 during measurement. The chemical composition of the LS and G2 was analyzed by X-ray  
125 fluorescence analysis (XRF) using a Philips PW 1830 instrument. The matrix composition of



126 G3 was provided by the IAEA and consisted of 96 wt%  $\text{CaSO}_4 \cdot 2\text{H}_2\text{O}$ , 1-2 wt%  $\text{P}_2\text{O}_5$ , 1.2 wt%  
 127  $\text{F}^-$ , 1 wt%  $\text{SiO}_2$  and 0.2 wt%  $\text{Al}_2\text{O}_3$  (Shakhashiro et al., 2011). The chemical composition of all  
 128 materials is summarized in Table 1.

129 **Table 1:** Chemical composition (in wt%) of LS, G1, G2 and G3

	LS	G1	G2	G3
CaO ( <i>C</i> )	51.1	41.2	45.9	39.5
SiO <sub>2</sub> ( <i>S</i> )	14.1	-	0.2	1.0
Al <sub>2</sub> O <sub>3</sub> ( <i>A</i> )	24.6	-	0.3	0.2
Fe <sub>2</sub> O <sub>3</sub> ( <i>F</i> )	0.5	-	-	-
SrO	-	-	0.8	-
MgO	3.8	-	0.2	-
SO <sub>3</sub> ( <i>S</i> )	0.4	58.8	51.4	56.5
TiO <sub>2</sub>	4.2	-	-	-
CeO <sub>2</sub>	-	-	0.3	-
P <sub>2</sub> O <sub>5</sub>	-	-	0.6	1.5
F <sup>-</sup>	-	-	-	1.2
Others	1.3	-	0.3	0.1

130

131 XRD analysis (D2 PHASER, Bruker) was performed to investigate the mineralogy of LS, G1,  
 132 G2 and G3. The X-ray tube was operated at 30 kV and 10 mA. Diffractograms were recorded  
 133 in continuous PSD fast mode between 5° and 70° 2θ at 0.02° step width with a counting time  
 134 of 0.3 s per step. As an internal standard, 10 wt% ZnO (99.9% purity, Merck) was added  
 135 (Jansen et al., 2011; Madsen et al., 2011). The samples were prepared using the back  
 136 loading technique and an anti-scatter slit was positioned 1 mm above the samples. During  
 137 acquisition, the samples were rotated at 15 rpm. The obtained data were evaluated with EVA  
 138 V.3.1 (Bruker AXS) software. For the quantitative analysis, MAUD (Lutterotti et al., 1999) was

139 used based on the Rietveld method (Rietveld, 1969). The results were recalculated from the  
 140 known ZnO content and are summarized in Table 2. During the time between sample  
 141 preparation by the IAEA and the use of G3, part of the gypsum has been transformed into  
 142 bassanite and anhydrite.

143 **Table 2:** Mineralogy (in wt%) of LS, G1, G2 and G3

	LS	G1	G2	G3
Calcio-olivine ( $\gamma-C_2S$ )	21.0	-	-	-
Tricalcium-aluminate ( $C_3A$ )	2.3	-	-	-
Mayenite ( $C_{12}A_7$ )	21.9	-	-	-
Periclase (MgO)	2.1	-	-	-
Perovskite ( $CaTiO_3$ )	1.3	-	-	-
Calcium aluminum magnesium silicate ( $Ca_{20}Al_{26}Mg_3Si_3O_{68}$ )	47.3	-	-	-
Gypsum ( $C\bar{S}.2H$ )	-	96.8	93.6	33.2
Bassanite ( $C\bar{S}.0.5H$ )	-	-	6.4	27.1
Anhydrite ( $C\bar{S}$ )	-	3.2	-	32.1
Amorphous	4.0	-	-	7.6

144

## 145 2.2 Sample preparation

146 A total of 7 paste samples (P0-P6) and 7 mortar samples (M0-M6) were prepared for  
 147 investigation. The precursor was composed of variable contents of LS, G1, G2 and G3. The  
 148 specific ratios for each sample are presented in Table 3. According to previous work (Nguyen  
 149 et al., 2019a), the content of gypsum was set at 30 wt%. Citric acid, supplied by Tokyo  
 150 Chemical Industry Co., Ltd., Japan (product code C1949), was used as a set retarder  
 151 (Nguyen et al., 2019b). The solution displayed a concentration of 0.5% citric acid and was

152 made by dissolving the solid in distilled water using magnetic stirring at a speed of 250 rpm  
 153 for 30 min at room temperature. Based on previous work (Nguyen et al., 2019a, 2019b), the  
 154 liquid-to-precursor ratio (L/P) was established at 0.45. For the preparation of the mortar  
 155 samples, CEN standard sand (DIN EN 196-1) was used with a sand-to-precursor ratio (S/P)  
 156 of 3 (European Committee for Standardization, 2016). Paste samples were prepared by  
 157 mixing the precursor and gradually adding the solution, followed by manually mixing for 3 min  
 158 to obtain good homogeneity. The mixing of mortar samples was performed in accordance  
 159 with EN 196-6 (European Committee for Standardization, 2010). After mixing, fresh pastes  
 160 were cast in silicon cubic molds of 35 mm × 35 mm × 35 mm, while mortars were cast in  
 161 steel molds with dimensions 40 mm × 40 mm × 160 mm according to EN 196-6 (European  
 162 Committee for Standardization, 2010). After casting, the molds were stored in sealed plastic  
 163 bags to avoid the loss of water. After 24 h, paste and mortar samples were removed from the  
 164 molds and were further cured under water at room temperature until testing.

165 **Table 3:** Precursor mixture ratios (in wt%)\*

	LS	G1	G2	G3
P0, M0	70	30	0	0
P1, M1	70	20	10	0
P2, M2	70	10	20	0
P3, M3	70	0	30	0
P4, M4	70	20	0	10
P5, M5	70	10	0	20
P6, M6	70	0	0	30

166 \*P0-P6 and M0-M6 refer to paste and mortar samples, respectively.

167

### 168 2.3 Methods

169 In order to study the heat evolution during hydration, isothermal calorimetry was performed  
170 on fresh pastes using a TAM Air Calorimeter at a set temperature of 25 °C during the first 8  
171 days of hydration. Paste samples were mixed ex-situ and poured into glass ampoules, which  
172 were then inserted into the calorimeter. The heat flow signal was recorded automatically  
173 every second during the period of measurement.

174 As for phase characterization, XRD data were collected from paste samples after 28 days of  
175 curing, using the same device, measurement set-up and analysis method as for the  
176 characterization of the raw materials (i.e., LS, G1, G2 and G3). After their curing period,  
177 paste samples were air-dried at room temperature whereafter they were manually milled in a  
178 porcelain mortar. Crystalline ZnO (purity 99.9%, Merck) was added to the samples as an  
179 internal standard by 10 wt%.

180 FTIR (Vertex 70, Bruker) was applied on paste samples after 28 days of curing to identify the  
181 bonding characteristics of the developed materials. Spectra were acquired in wavenumber  
182 ranges from 4000  $\text{cm}^{-1}$  to 600  $\text{cm}^{-1}$ , at a resolution of 4  $\text{cm}^{-1}$  and with 32 scans per  
183 measurement, supported by Opus software. The spectra were collected in ATR (attenuated  
184 total reflection) mode, using a diamond/ZnSe crystal with single interaction (PIKE  
185 Technologies Inc.). Prior to measurement, a background spectrum was recorded. In addition,  
186 TGA (Precisa prepASH 129) was carried out on paste samples after 28 days of curing, by  
187 heating the samples from 25 °C to 1000 °C under  $\text{N}_2$  atmosphere, with a heating rate of 5  
188 °C/min. Sample preparation for FTIR and TGA was the same as for XRD.

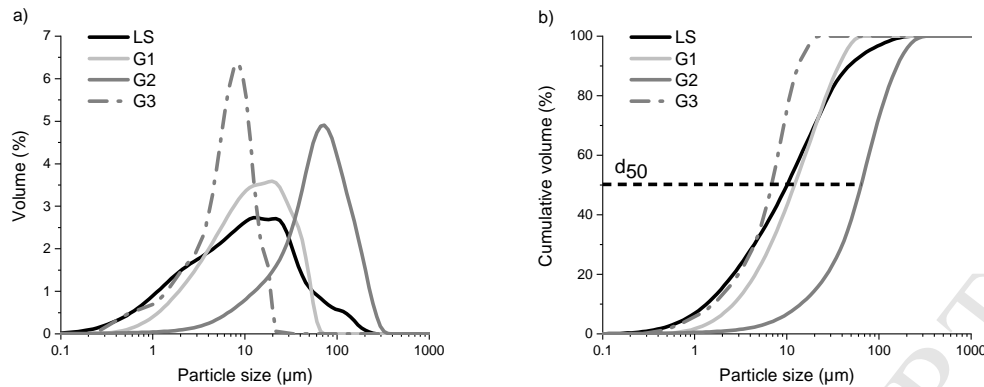
189 Compressive strength tests on mortar samples were undertaken in triplicate after 7, 28 and  
190 90 days of curing on a Zwick Z100 or a Dartec with a load cell of 100 or 400 kN, respectively.  
191 SEM (Zeiss Sigma) was used to observe the morphology of the fracture surface of mortar  
192 samples after 7 and 28 days of curing after compressive strength testing. SEM samples were  
193 coated with 70 nm Pt prior to the observation. Images were collected in secondary electron  
194 (SE) mode with 5 kV acceleration voltage and a working distance of about 5 mm.

195

### 196 3. Results and discussion

#### 197 3.1. Particle size distribution

198 The particle size distribution of the used materials is presented in Fig. 1; a unimodal  
199 distribution is the result in each case. LS was characterized by particle sizes ranging from 0.1  
200  $\mu\text{m}$  to 223  $\mu\text{m}$ , while the range for G1 was narrower, i.e., from 0.2  $\mu\text{m}$  to 66  $\mu\text{m}$ . The particle  
201 size of the Finnish PG (G2) was significantly larger compared with the Polish PG (G3). G2  
202 consisted of particles with sizes ranging from 0.1  $\mu\text{m}$  to 324  $\mu\text{m}$ , with most particles ranging  
203 from approximately 20  $\mu\text{m}$  to 200  $\mu\text{m}$ . The particle size of G3 ranged from 0.2  $\mu\text{m}$  to 24  $\mu\text{m}$ ,  
204 with the highest particle population in the range from 2  $\mu\text{m}$  to 20  $\mu\text{m}$ . These data indicate that  
205 the average particle size of G3 was almost 10 times lower than the average particle size of  
206 G2. The  $d_{50}$  value for LS, G1, G2 and G3 was 10  $\mu\text{m}$ , 12  $\mu\text{m}$ , 66  $\mu\text{m}$  and 7  $\mu\text{m}$ , respectively.  
207 Differences in particle size distribution can have a significant influence on the hydration  
208 kinetics and microstructural development, and consequently on the final properties of the  
209 material (Liu et al., 2016). The L/P was established at 0.45 for all samples, although a  
210 decline in paste workability was observed upon substituting G1 by G3 (P4-P6); the use of the  
211 coarser G2 (P1-P3) slightly enhanced the workability. A lower particle size distribution needs  
212 more water for a given flowability because its higher specific surface area increases the  
213 water-absorption capacity and the interparticle forces, while finer particles hydrate also faster  
214 than coarser ones (Jiao et al., 2017; Roussel et al., 2010; Wallevik, 2009). The choice to not  
215 additionally mill G2 was based on our intention to restrict the overall production cost and  
216 energy investment of a future full-scale application. However, in future studies it is worth  
217 investigating how simple pre-treatment methods (e.g. milling) affect the workability and  
218 mechanical properties of mixtures.



219

220 **Figure 1:** Particle size distribution of LS, G1, G2 and G3: a) volume and b) cumulative  
 221 volume

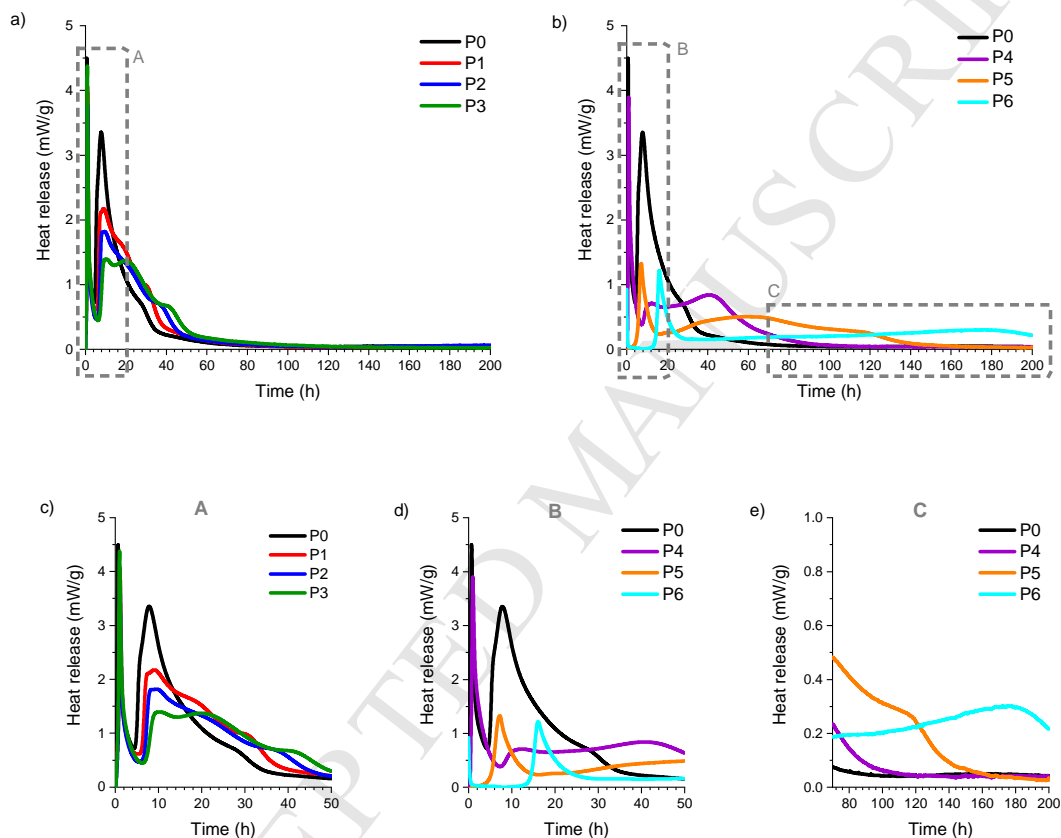
222

### 223 3.2. Heat of hydration via isothermal calorimetry

224 The heat release during the hydration of paste samples was monitored by isothermal  
 225 calorimetry and is presented in Fig. 2. The reaction between LS and G1 (P0) is manifested  
 226 by an initial wetting and dissolution peak, followed by a main hydration peak 8 h after the  
 227 start of the measurement. This high-intensity peak is attributed to the formation of ettringite,  
 228 followed by a shoulder at around 28 h designating (1) secondary ettringite formation (Nguyen  
 229 et al., 2019a), (2) the conversion of ettringite to monosulfate (Kirchheim et al., 2018) and/or  
 230 (3) the densification of the C-S-H phase. The intensity of the initial wetting and dissolution  
 231 peak is comparable for all samples, irrespective of the gypsum source used. The gradual  
 232 substitution of gypsum by Finnish PG (i.e., P1-P3) decreased the heat release for the main  
 233 hydration peak. The reaction rate was not affected, however, as the timing of these main  
 234 hydration peaks did not shift. When gypsum is substituted by Polish PG (i.e., P4-P6), the  
 235 height of the main hydration peak decreases and this peak is shifted in time (i.e., it occurs at  
 236 11 h for P4, 7 h for P5 and 16 h for P6). Interestingly, a dormant period occurs between the  
 237 main hydration peak and the shoulder. This period increases when Polish PG content is  
 238 increased. This may be due to an increased level of impurities in the precursor when the  
 239 proportion of PG increases (Huang et al., 2016). The shoulder peaks at 42, 60 and 180 h for

240 P4, P5 and P6, respectively. Along with the presence of impurities in PG, the differences in  
241 particle size distribution may also contribute to the shifted heat evolution (Liu et al., 2016). In  
242 addition to  $\text{CaSO}_4 \cdot 2\text{H}_2\text{O}$ , the Finnish PG also contains remnants of phosphoric acid, SrO and  
243  $\text{CeO}_2$ . Phosphoric acid is known as a setting retarder for cement, as already extensively  
244 described in the literature ((Rashad, 2017) and references therein). However, the content of  
245 phosphoric acid in the Polish phosphogypsum (1-2 wt%) is almost 2 times higher compared  
246 with the Finnish PG (0.6 wt%). For this reason, the influence on the kinetics of the hydration  
247 reaction was greater for P4, P5 and P6, where the delay in reaction is directly proportional to  
248 the amount of gypsum substituted. In cementitious matrices,  $\text{Sr}^{2+}$  ions are immobilized due to  
249 the substitution of  $\text{Ca}^{2+}$  in the ettringite structure and by sorption on the C-(A)-S-H phase,  
250 while a small proportion of  $\text{Sr}^{2+}$  ions precipitates as  $\text{SrOH}^+$  (Abdel Rahman et al., 2013).  $\text{Ce}^{3+}$   
251 is expected to precipitate as insoluble  $\text{CeO}_2$  or  $\text{Ce}(\text{OH})_3$  at alkaline pH, although  
252 incorporation into the ettringite and/or C-(A)-S-H phases may also be expected.  $\text{F}^-$   
253 precipitates as insoluble  $\text{CaF}_2$  in alkaline cementitious matrices (Park et al., 2008; Silveira et  
254 al., 2003) while it may also be incorporated in the ettringite phase or other mineral phases  
255 (e.g. fluorellestadite) (Gomes et al., 2012; He and Suito, 2008). The initial rapid precipitation  
256 of insoluble species such as  $\text{SrOH}^+$ ,  $\text{CeO}_2$ ,  $\text{Ce}(\text{OH})_3$  and  $\text{CaF}_2$  is expected to decrease the  
257 heat release, by decreasing the available reactive surface of the precursor. Regarding P1,  
258 P2 and P3, it is likely that both (1) the presence of SrO,  $\text{CeO}_2$  and phosphoric acid in G2 and  
259 (2) the higher particle size of G2 decreased the degree of reaction (i.e., the peak height). For  
260 P4, P5 and P6 both the decrease in the degree of reaction and the prolonged reaction rate  
261 may be due to the presence of  $\text{F}^-$  and phosphoric acid in G3, while it is also reasonable that  
262 both phenomena are being influenced by the small particle size of G3 (Liu et al., 2016),  
263 whereby a portion of the precursor gets covered by a rapid initial hydration product formation.  
264 It is also important to note that the sulfate sources showed variable mineralogy (i.e., a  
265 combination of gypsum, bassanite and/or anhydrite) which could also have influenced the  
266 hydration rate (Chandara et al., 2009; Pelletier-Chaignat et al., 2011). The rapid hydration of  
267 bassanite (for P4, P5 and P6) is not clearly distinguishable because the heat flow curves are

268 the summation of heat released and consumed by various reactions that occur in sequence  
 269 and/or in parallel during hydration. However, the notably prolonged shoulder for P4, P5 and  
 270 P6 could be attributed to the slower anhydrite hydration. The kinetics of ettringite formation  
 271 can influence its microstructural appearance, in which a fast reaction results in poorly-  
 272 crystallized phases and a slower reaction results in a well-crystallized needle structure (Allevi  
 273 et al., 2016).

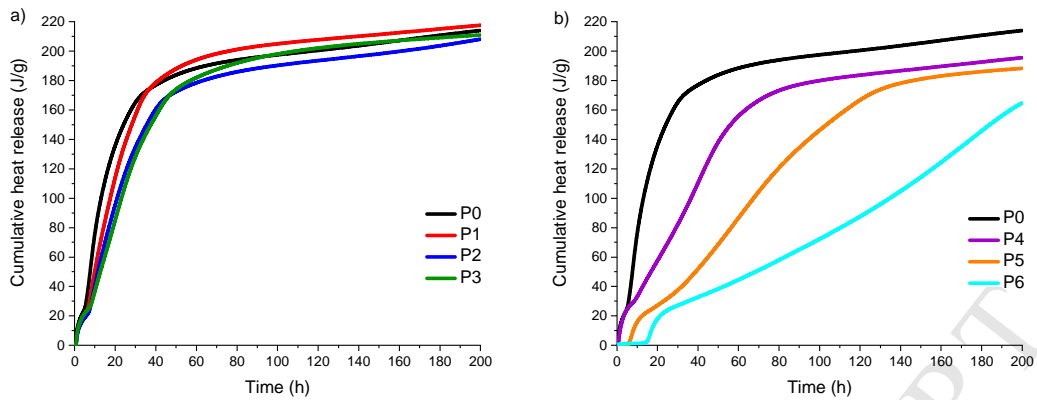


274

275

276 **Figure 2:** Heat release of mixtures incorporating a) G2 (i.e., P1-P3), b) G3 (i.e., P4-P6) in  
 277 comparison with the reference mixture P0, and the magnification of region c) A, d) B and e)  
 278 C of the heat evolution





279

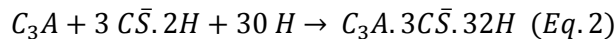
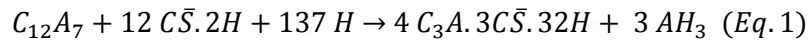
280 **Figure 3:** Cumulative heat release of mixtures incorporating a) G2 (i.e., P1-P3) and b) G3  
 281 (i.e., P4-P6) in comparison with the reference mixture P0

282 The cumulative heat release is shown in Fig. 3. The use of PG's of different origin resulted in  
 283 variable curve shapes. The gradual substitution of gypsum by Finnish PG (Fig. 3a)  
 284 decreased the heat release during the first 40 h of hydration proportionally. Thereafter, the  
 285 curves for P0, P1, P2 and P3 became quite similar, obtaining a cumulative heat of  
 286 approximately 200 J/g after 200 h of hydration. From Fig. 3b it is clear that the substitution of  
 287 gypsum by the Polish PG decreases and delays the heat release proportional to the  
 288 substitution degree. The cumulative heat release after 200 h for P4, P5 and P6 is 195 J/g,  
 289 188 J/g and 164 J/g, respectively. From the slope of the curves it is concluded that the  
 290 hydration of the pastes is still ongoing even after 200 h. The question remains to what extent  
 291 the decreased and delayed reaction rate during the first 200 h has an influence on the final  
 292 hydration products and properties of the material. This is investigated in the sections below.

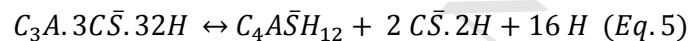
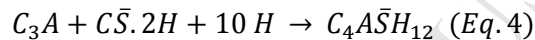
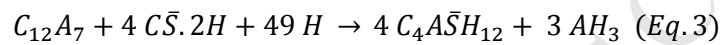
293

### 294 3.3. X-ray diffraction

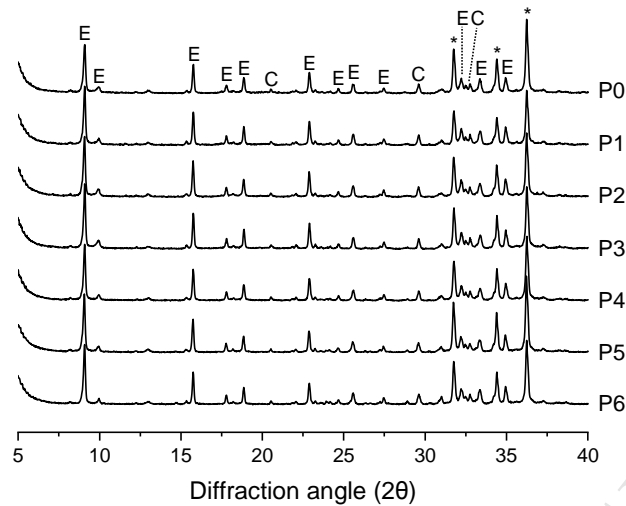
295 The X-ray diffractograms, obtained after 28 days of curing, are depicted in Fig. 4 from 5° to  
 296 40° 2θ. As already described in previous work (Nguyen et al., 2019a, 2019b), ettringite  
 297 ( $C_3A \cdot 3\bar{C}\bar{S} \cdot 32H$ ) is the main crystalline phase produced upon the reaction between mayenite  
 298 and gypsum (Eq. 1), and tricalcium-aluminate and gypsum (Eq. 2):



299 Depending on the reactivity of the calcium sulfate source, the water content, the depletion of  
 300 calcium and sulfate by rapid ettringite formation and the pH, monosulfate ( $C_4A\bar{S}H_{12}$ ) can be  
 301 generated in sequence or in parallel from the hydration between mayenite and gypsum (Eq.  
 302 3) and tricalcium-aluminate and gypsum (Eq. 4), or from the conversion of ettringite to  
 303 monosulfate (Eq. 5) (Winnefeld and Lothenbach, 2010).



304 In most cases, however, monosulfate has a very low crystallinity and is therefore hard to  
 305 detect by XRD (Gastaldi et al., 2016; Le Saout et al., 2004; Matschei et al., 2007).  
 306 Aluminium-hydroxide ( $AH_3$ ), a minor hydration product generated both in the reaction  
 307 between mayenite and gypsum to form ettringite (Eq. 1) and in the reaction between  
 308 mayenite and gypsum to form monosulfate (Eq. 3), is also ascribed to the amorphous part  
 309 (Gastaldi et al., 2016; Qoku et al., 2017). The presence of Si from the calcio-olivine phase in  
 310 the LS gives rise to amorphous C-S-H generation. Therefore, FTIR and TGA are useful  
 311 complementary techniques to carry out in parallel with XRD. The aforementioned reactions  
 312 (Eq. 1 - Eq. 5 and C-S-H generation) are expected to be the main hydration reactions,  
 313 although this list is not exhaustive, e.g. minor hydration products linked to impurities such as  
 314 fluoride (Jun et al., 2001; Pajares et al., 2002) and phosphorus (Huang et al., 2016) can also  
 315 be formed. From Fig. 4, the main crystalline phases recognized are ettringite ("E") and calcio-  
 316 olivine ("C"). The peaks of zincite are indicated with an asterisk.



317

318 **Figure 4:** XRD diffractograms of all paste mixtures after 28 days of curing

319 Quantification of the amorphous and crystalline phases was performed using the Rietveld  
 320 method (Rietveld, 1969) and is presented in Fig. 5a. The highest amorphous content was  
 321 found for P0 (71.8 wt%), which decreased upon the substitution of G1 by G2 and G3. The  
 322 ettringite content was comparable for all samples and ranged from 17.9 to 22.4 wt%. Small  
 323 amounts of braunite (0.3 – 2.0 wt%) and jasmundite (< 0.5 wt%) were identified as crystalline  
 324 hydration products. In Fig. 5b, only the phases originating from the precursor are presented.  
 325 The dissolution grade of the LS was significantly lower when PG was used instead of G1,  
 326 likely due to the impurities from PG. For P0, neither gypsum, bassanite nor anhydrite were  
 327 detected. For P1-P3, small amounts of gypsum (0.1 - 0.3 wt%), bassanite (0.4 - 0.6 wt%) and  
 328 anhydrite (< 0.3 wt%) were identified. For P4-P6, only bassanite (< 0.4 wt%) and anhydrite  
 329 (0.3 - 0.5 wt%) were discovered. It has to be noted here that the gypsum in P1-P3 may also  
 330 be (partly) secondary gypsum, generated according to Eq. 5.

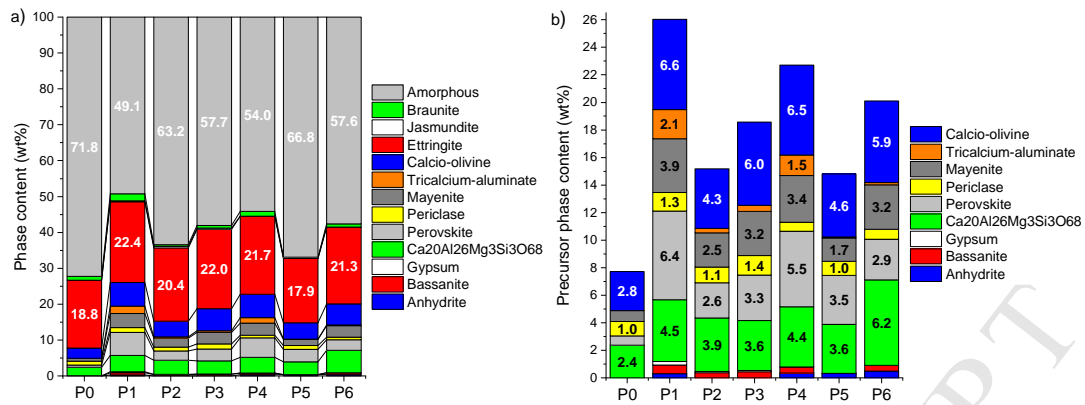
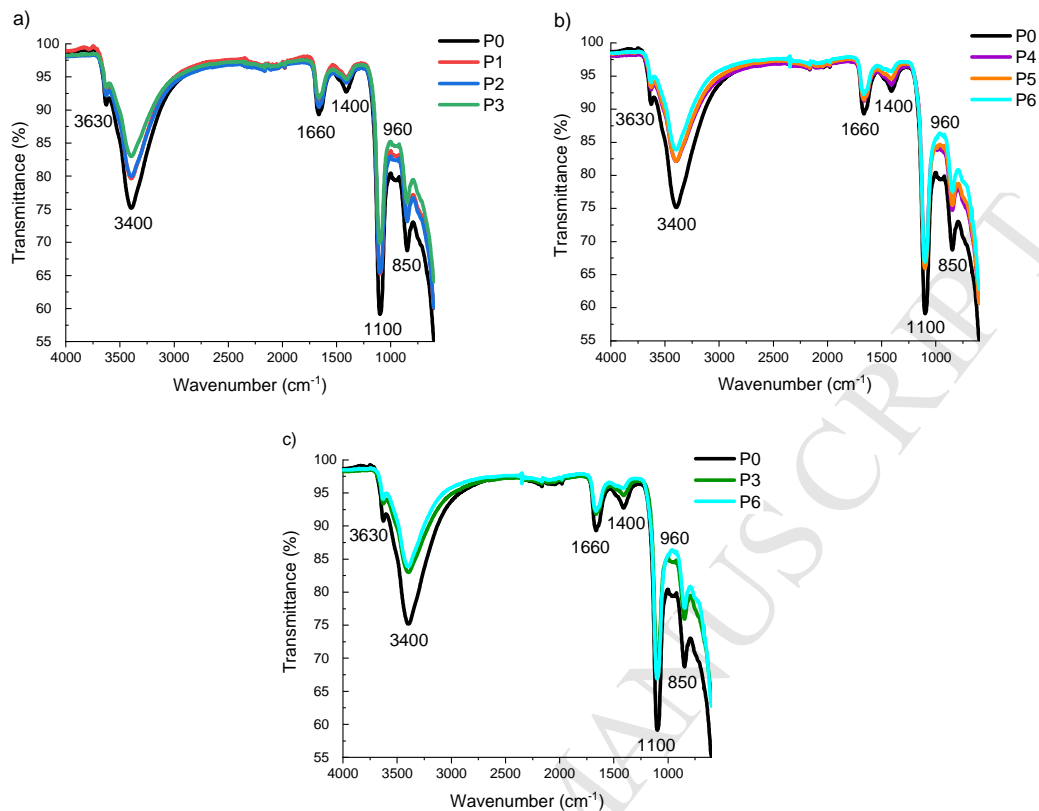


**Figure 5:** Q-XRD after 28 days of curing: a) phase content of all paste mixtures and b) the content of leftover phases from the precursor (i.e., LS and (phospho-)gypsum) in these mixtures

### 3.4. Fourier-transform infrared spectroscopy

FTIR spectra were recorded from paste samples after 28 days of curing. Curves are shown in Fig. 6. The bands noted at  $3630\text{ cm}^{-1}$ ,  $3400\text{ cm}^{-1}$  and  $1660\text{ cm}^{-1}$  are assigned to crystalline-bound water. The C-O bonding is deduced from the bands at  $1400\text{ cm}^{-1}$  and  $850\text{ cm}^{-1}$ . The Al-O-H bonding is recognized from the band at around  $960\text{ cm}^{-1}$  and the S-O stretching occurs at  $1100\text{ cm}^{-1}$  (Scholtzová et al., 2015). Whether or not these bands are induced by ettringite, monosulfate or aluminium-hydroxide is uncertain. However, in each case the intensity of these bands is higher for P0 and decreases upon substituting gypsum by PG, which could imply that fewer species were available for hydration product formation. This hypothesis would agree with Q-XRD in Fig. 5. Since the bands typical for Si-O bonding are overlapping, no firm conclusions can be drawn for the C-S-H phase. The bands from the C-O bonding could be related to (1) carbonation that has occurred during drying and milling of the pastes, and/or (2) the presence of thaumasite next to ettringite. However, carbonation was not observed in XRD, so it has occurred during sample preparation. Nevertheless, it was reduced when PG was used. From Fig. 6c, it is concluded that the spectra for P3 and P6 are generally quite similar (consistent with Q-XRD in Fig. 5), while the presence of the C-O

352 bonding is lowest when the Polish PG was used (P6).



353

354

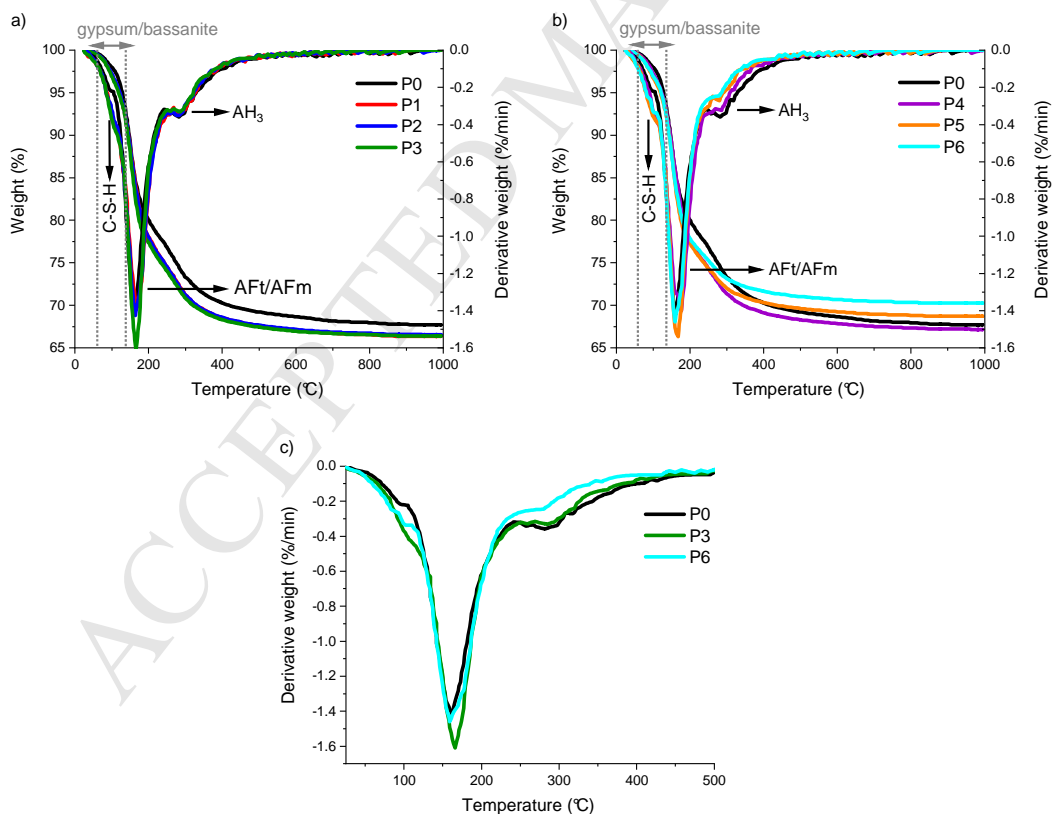
355 **Figure 6:** FTIR spectra of mixtures incorporating a) G2 (i.e., P1-P3), b) G3 (i.e., P4-P6) in  
 356 comparison with the reference mixture P0, and c) the comparison among P0, P3 and P6

357

### 358 3.5. Thermogravimetric analysis

359 The graphs of TGA and the derivative thermogravimetric (DTG) curves are presented in Fig.  
 360 7. From the endothermic peak around 110 °C, the existence of the amorphous C-S-H phase  
 361 is detected (Trauchessec et al., 2015). The largest endothermic peak from 150 to 180 °C is  
 362 assigned to the decomposition of ettringite (Gaviria et al., 2018). The existence of  
 363 monosulfate and aluminium-hydroxide can be deduced from the peaks located at around 180  
 364 to 200 °C and 200 to 300 °C, respectively (Qoku et al., 2017). The presence of gypsum (and  
 365 bassanite) can be deduced from the region between 90 and 140 °C (Chang et al., 1999; Lou  
 366 et al., 2011; Yu and Brouwers, 2012). Less aluminium-hydroxide was generated when the

367 Polish PG was incorporated (P4-P6), compared with P0. This means that (1) the formation of  
 368 ettringite by Eq. 2 was more dominant than that by Eq. 1 and/or (2) the aluminium-hydroxide  
 369 gets incorporated into the C-S-H gel resulting in a calcium-aluminosilicate-hydrate (C-A-S-H)  
 370 phase. Both phenomena could result from slower kinetics compared with P0 (see Fig. 3b).  
 371 From Fig. 7c it is concluded that the use of Finnish PG increases the monosulfate content  
 372 compared with P0 (gypsum) and P6 (Polish PG). Since the aluminium-hydroxide content is  
 373 not affected by the substitution of gypsum by Finnish PG (P1-P3), it is expected that the  
 374 monosulfate generation is mainly carried out by Eq. 4 and Eq. 5. Consequently, it is possible  
 375 that the formation of secondary gypsum by Eq. 5 (consistent with Q-XRD), together with  
 376 remnants of bassanite have a cumulative effect on the region from 90 to 140 °C (and thus  
 377 the C-S-H peak). After 28 days of curing, P3 contained 0.1 wt% gypsum and 0.4 wt%  
 378 bassanite; P6 contained no gypsum and 0.4 wt% bassanite.

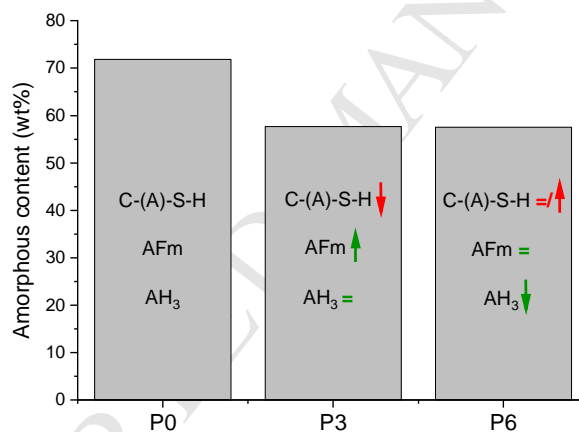


379

380

381 **Figure 7:** TGA and DTG curves of mixtures incorporating a) G2 (i.e., P1-P3), b) G3 (i.e., P4-  
 382 P6) in comparison with the reference mixture P0, and c) the comparison among P0, P3 and  
 383 P6

384 For P3, due to (1) secondary gypsum, (2) remnants of bassanite, (3) comparable ettringite  
 385 and aluminium-hydroxide content and (4) an increased monosulfate content, the C-(A)-S-H  
 386 content is lower compared with P0. For P6, it is expected that due to (1) unreacted  
 387 bassanite, (2) comparable ettringite and monosulfate content and (3) a decreased  
 388 aluminium-hydroxide content, the C-(A)-S-H content is equal or even slightly increased  
 389 compared with P0. These expected changes in the amorphous phases are depicted in Fig. 8;  
 390 the total amorphous content is derived from Q-XRD.



391

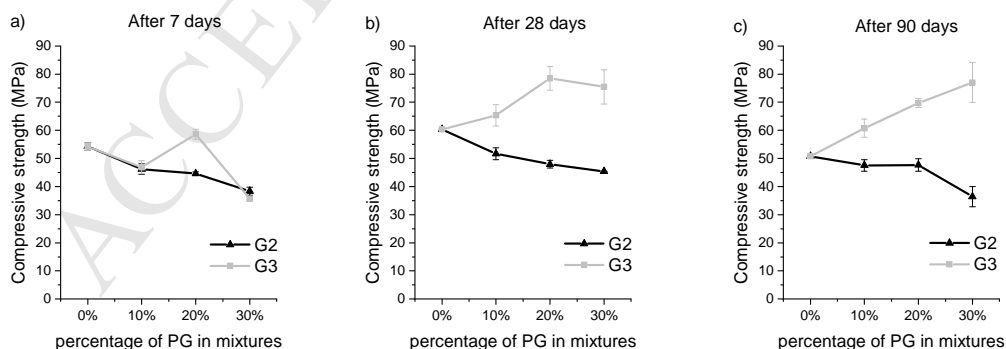
392 **Figure 8:** Expectations of amorphous phase changes (in green, what is known; in red, what  
 393 is expected)

394

### 395 3.6. Compressive strength

396 In Fig. 9, the compressive strength after 7, 28 and 90 days of curing is presented. Upon the  
 397 substitution of gypsum by Finnish PG (i.e., G2), the compressive strength is lowered and this  
 398 reduction is in proportion to the amount of PG incorporated. In addition, mixtures with G2

399 developed full compressive strength after 7 days of curing, with negligible strength  
 400 development in the period from 7 to 90 days of curing. This result is in good agreement with  
 401 other ettringite-based binders reported as high early-age strength binders (Kim et al., 2016;  
 402 Quillin, 2001). In contrast, the substitution of gypsum by the Polish PG (i.e., G3) increases  
 403 the compressive strength considerably in the long term. Under the effects of impurities in G3,  
 404 the strength development was delayed. The mortar samples attained their final strength after  
 405 28 days of curing, while there was no significant change in the compressive strength of these  
 406 mortars when comparing the results after 28 and 90 days of curing. It is worth noting that,  
 407 despite the delayed heat evolution of P5 (compared with P0) (Fig. 3b), M5 showed increased  
 408 compressive strength (compared with M0) even after 7 days of curing. This is presumed to  
 409 be a consequence of a better particle packing due to the smaller particle size of G3. In  
 410 contradiction to the negative effects of impurities from PG on the strength of cementitious  
 411 binders reported in (Akin Altun and Sert, 2004; Shen et al., 2014; Smadi et al., 1999), the use  
 412 of G3 in LSG offered an increase of up to 60% in compressive strength. This is likely due to  
 413 the late reactions, the fine particle size of G3, which led to a denser LSG matrix, and  
 414 changes in the crystalline and amorphous phase composition, as shown in Fig. 5 and Fig. 8,  
 415 respectively. In addition, nitrogen adsorption/desorption tests were carried out in a parallel  
 416 paper (Gijbels et al., 2019).



417

418 **Figure 9:** Compressive strength ( $1\sigma$  error) of mixtures incorporating G2 and G3 after a) 7, b)

419

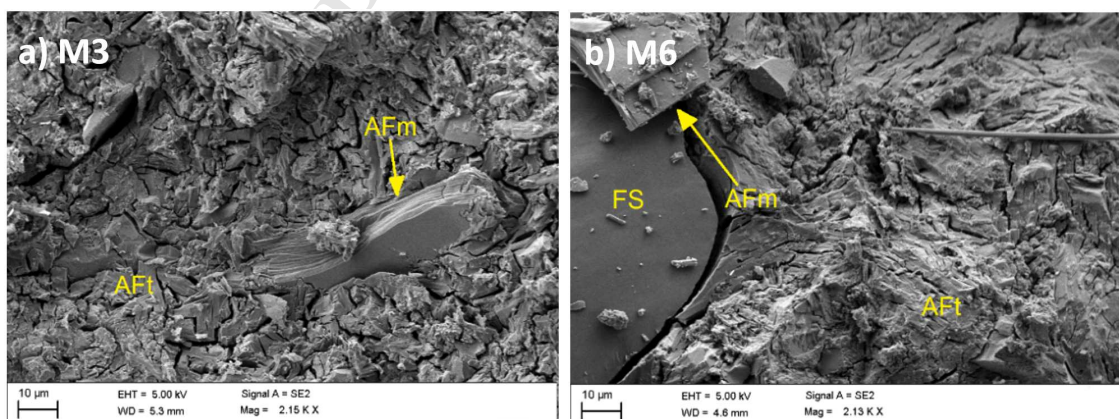
28 and c) 90 days of curing



420

421 **3.7. Morphological analysis**

422 The fracture surface (after compressive strength testing) of mortar samples was investigated  
423 by SEM after 7 and 28 days of curing. Fig. 10 shows the SEM images of M3 and M6 after 28  
424 days of curing, which represent the worst and the best combination in terms of compressive  
425 strength. It is clear that the main phase is ettringite (indicated as AFt in Fig. 10) for all  
426 mixtures from the reaction between LS and PG (Eq. 1-2). The phase was embedded in an  
427 amorphous matrix intermixed with undissolved LS particles and sand (indicated as FS in Fig.  
428 10). In addition, the monosulfate phase (indicated as AFm in Fig. 10) has a layered structure  
429 consisting of positively charged layers balanced by water and anions in the interlayer  
430 (Baquerizo et al., 2015). As reported in e.g. (Gastaldi et al., 2016; Le Saout et al., 2004;  
431 Matschei et al., 2007), monosulfate is also a semi-ordered structure and hence can stay in  
432 the amorphous phase along with aluminium-hydroxide and C-(A)-S-H. Consequently, there  
433 was no monosulfate detected in the diffractograms shown in Fig. 4. Furthermore, the  
434 morphology of M6 exhibited a denser structure than that of M3 leading to higher compressive  
435 strength, which is likely due to a better particle packing and more pronounced hydration at a  
436 later age.



437

438 **Figure 10:** SEM images of a) M3 and b) M6 after 28 days of curing

439

#### 440 **4. Conclusions**

441 This study investigated the potential use of Finnish (G2) and Polish PG (G3) as a potential  
442 calcium sulfate source for the production of LSGs. The results were compared with a  
443 reference LSG from pure gypsum (G1). During the first hours of hydration, the heat flow was  
444 decreased and delayed upon using PG, and these effects were more pronounced when  
445 using Polish PG. After 28 days of curing, the main crystalline phase in all binders was  
446 ettringite (17.9 to 22.4 wt%), while the amorphous content was variable (ranging from 49.1 to  
447 71.8 wt%), and was reduced when PG was incorporated, irrespective of its origin. The use of  
448 Finnish PG increased the monosulfate content and encouraged the formation of secondary  
449 gypsum, while it lowered the C-(A)-S-H content compared to the reference LSG. Upon using  
450 Polish PG, the aluminium-hydroxide content was diminished, while the monosulfate content  
451 was similar to the reference LSG, and the C-(A)-S-H content was equal or potentially even  
452 increased. The substitution of gypsum by Finnish PG reduced the compressive strength by  
453 30% after 90 days of curing, compared with the reference LSG. However, when pure gypsum  
454 was replaced by Polish PG, the compressive strength increased by 60% after 90 days. This  
455 investigation revealed that the combination of LS and PG can effectively produce an almost  
456 entirely by-product-based binder.

457

458 **Declarations of interest:** none

459

#### 460 **Acknowledgements**

461 This work was supported by the Fund for Scientific Research Flanders (FWO). The authors  
462 would like to acknowledge the networking support of the COST Action TU1301,  
463 [www.norm4building.org](http://www.norm4building.org). At the University of Oulu, this work was done as part of the FLOW  
464 Project (project number 8904/31/2017) funded by Business Finland in the ERA-MIN 2  
465 Innovation program (EU Horizon 2020 program). SSAB Europe Oy and Yara Oy are

466 acknowledged for providing ladle slag and phosphogypsum, respectively.

467

## 468 References

- 469 Abdel Rahman, R.O., Zin El Abidin, D.H.A., Abou-Shady, H., 2013. Assessment of strontium  
470 immobilization in cement-bentonite matrices. *Chem. Eng. J.* 228, 772–780.  
471 <https://doi.org/10.1016/j.cej.2013.05.034>
- 472 Akin Altun, I., Sert, Y., 2004. Utilization of weathered phosphogypsum as set retarder in  
473 Portland cement. *Cem. Concr. Res.* 34, 677–680.  
474 <https://doi.org/10.1016/j.cemconres.2003.10.017>
- 475 Al-Hwaiti, M.S., 2015. Assessment of the radiological impacts of treated phosphogypsum  
476 used as the main constituent of building materials in Jordan. *Environ. Earth Sci.* 74,  
477 3159–3169. <https://doi.org/10.1007/s12665-015-4354-2>
- 478 Allevi, S., Marchi, M., Scotti, F., Bertini, S., Cosentino, C., 2016. Hydration of calcium  
479 sulphoaluminate clinker with additions of different calcium sulphate sources. *Mater.*  
480 *Struct. Constr.* 49, 453–466. <https://doi.org/10.1617/s11527-014-0510-5>
- 481 ASTM International, 2017. ASTM C204-17. Standard test methods for fineness of hydraulic  
482 cement by air-permeability apparatus.
- 483 Baquerizo, L.G., Matschei, T., Scrivener, K.L., Saeidpour, M., Wadsö, L., 2015. Hydration  
484 states of AFm cement phases. *Cem. Concr. Res.* 73, 143–157.  
485 <https://doi.org/10.1016/j.cemconres.2015.02.011>
- 486 Cánovas, C.R., Macías, F., Pérez-López, R., Basallote, M.D., Millán-Becerro, R., 2018.  
487 Valorization of wastes from the fertilizer industry: Current status and future trends. *J.*  
488 *Clean. Prod.* 174, 678–690. <https://doi.org/10.1016/j.jclepro.2017.10.293>
- 489 Chandara, C., Azizli, K.A.M., Ahmad, Z.A., Sakai, E., 2009. Use of waste gypsum to replace  
490 natural gypsum as set retarders in portland cement. *Waste Manag.* 29, 1675–1679.  
491 <https://doi.org/10.1016/j.wasman.2008.11.014>
- 492 Chang, H., Huang, P.J., Hou, S.C., 1999. Application of thermo-Raman spectroscopy to  
493 study dehydration of  $\text{CaSO}_4 \cdot 2\text{H}_2\text{O}$  and  $\text{CaSO}_4 \cdot 0.5\text{H}_2\text{O}$ . *Mater. Chem. Phys.* 58, 12–  
494 19. [https://doi.org/10.1016/S0254-0584\(98\)00239-9](https://doi.org/10.1016/S0254-0584(98)00239-9)
- 495 Council of the European Union, 2014. Council directive 2013/59/EURATOM, European Basic  
496 Safety Standards (BSS) for Protection against Ionising Radiation. *Off. J. Eur. Union L*  
497 13/1.
- 498 European Committee for Standardization, 2016. EN 196-1. Methods of testing cement - Part  
499 1: Determination of strength.
- 500 European Committee for Standardization, 2012. EN 450-1: Fly ash for concrete - Part 1:  
501 Definition, specifications and conformity criteria.
- 502 European Committee for Standardization, 2010. EN 196-6. Methods of testing cement - Part  
503 6: Determination of fineness.
- 504 Gastaldi, D., Paul, G., Marchese, L., Irico, S., Boccaleri, E., Mutke, S., Buzzi, L., Canonico,  
505 F., 2016. Hydration products in sulfoaluminate cements: Evaluation of amorphous  
506 phases by XRD/solid-state NMR. *Cem. Concr. Res.* 90, 162–173.  
507 <https://doi.org/10.1016/j.cemconres.2016.05.014>

- 508 Gaviria, X., Borrachero, M.V., Payá, J., Monzó, J.M., Tobón, J.I., 2018. Mineralogical  
509 evolution of cement pastes at early ages based on thermogravimetric analysis (TG). *J.*  
510 *Therm. Anal. Calorim.* 132, 39–46. <https://doi.org/10.1007/s10973-017-6905-0>
- 511 Gijbels, K., Nguyen, H., Kinnunen, P., Samyn, P., Schroyers, W., Pontikes, Y., Schreurs, S.,  
512 Illikainen, M., 2019. Radiological and leaching assessment of an ettringite-based mortar  
513 from ladle slag and phosphogypsum (submitted in May 2019, currently under review).  
514 *Cem. Concr. Res.*
- 515 Gomes, A.F.S., Lopez, D.L., Ladeira, A.C.Q., 2012. Characterization and assessment of  
516 chemical modifications of metal-bearing sludges arising from unsuitable disposal. *J.*  
517 *Hazard. Mater.* 199–200, 418–425. <https://doi.org/10.1016/j.jhazmat.2011.11.039>
- 518 Hammas-Nasri, I., Horchani-Naifer, K., Férid, M., Barca, D., 2019. Production of a rare  
519 earths concentrate after phosphogypsum treatment with dietary NaCl and Na<sub>2</sub>CO<sub>3</sub>  
520 solutions. *Miner. Eng.* 132, 169–174. <https://doi.org/10.1016/j.mineng.2018.12.013>
- 521 He, H., Suito, H., 2008. Immobilization of fluorine in aqueous solution by calcium aluminum  
522 ferrite and the mixture of calcium aluminate and gypsum. *ISIJ Int.* 42, 794–799.  
523 <https://doi.org/10.2355/isijinternational.42.794>
- 524 Huang, Y., Qian, J., Liang, J., Liu, N., Li, F., Shen, Y., 2016. Characterization and  
525 calorimetric study of early-age hydration behaviors of synthetic ye'elimité doped with the  
526 impurities in phosphogypsum. *J. Therm. Anal. Calorim.* 123, 1545–1553.  
527 <https://doi.org/10.1007/s10973-015-5009-y>
- 528 International Atomic Energy Agency (IAEA), 2013. Radiation Protection and Management of  
529 NORM Residues in the Phosphate Industry, Safety Reports Series No. 78. IAEA,  
530 Vienna. <https://doi.org/10.1016/j.resourpol.2012.04.002>
- 531 International Organization for Standardization (ISO), 2009. ISO 13320:2009 - Particle size  
532 analysis: Laser diffraction methods.
- 533 Jansen, D., Stabler, C., Goetz-Neunhoeffer, F., Dittrich, S., Neubauer, J., 2011. Does  
534 Ordinary Portland Cement contain amorphous phase? A quantitative study using an  
535 external standard method. *Powder Diffr.* 26, 31–38. <https://doi.org/10.1154/1.3549186>
- 536 Jiao, D., Shi, C., Yuan, Q., An, X., Liu, Y., Li, H., 2017. Effect of constituents on rheological  
537 properties of fresh concrete-A review. *Cem. Concr. Compos.* 83, 146–159.  
538 <https://doi.org/10.1016/j.cemconcomp.2017.07.016>
- 539 Jun, C., Xin, C., Futian, L., Lingchao, L., Bing, T., 2001. Influence of fluorite on the Ba-  
540 bearing sulphoaluminate cement. *Cem. Concr. Res.* 31, 213–216.  
541 [https://doi.org/10.1016/S0008-8846\(00\)00450-6](https://doi.org/10.1016/S0008-8846(00)00450-6)
- 542 Kim, J.M., Choi, S.M., Han, D., 2016. Improving the mechanical properties of rapid air cooled  
543 ladle furnace slag powder by gypsum. *Constr. Build. Mater.* 127, 93–101.  
544 <https://doi.org/10.1016/j.conbuildmat.2016.09.102>
- 545 Kirchheim, A.P., Rodríguez, E.D., Myers, R.J., Gobbo, L.A., Monteiro, P.J.M., Dal Molin,  
546 D.C.C., de Souza, R.B., Cincotto, M.A., 2018. Effect of gypsum on the early hydration of  
547 cubic and Na-doped orthorhombic tricalcium aluminate. *Materials (Basel)*. 11, 1–17.  
548 <https://doi.org/10.3390/ma11040568>
- 549 Koopman, C., Witkamp, G.J., 2002. Ion exchange extraction during continuous  
550 recrystallization of CaSO<sub>4</sub> in the phosphoric acid production process: Lanthanide  
551 extraction efficiency and CaSO<sub>4</sub> particle shape. *Hydrometallurgy* 63, 137–147.  
552 [https://doi.org/10.1016/S0304-386X\(01\)00219-5](https://doi.org/10.1016/S0304-386X(01)00219-5)
- 553 Le Saout, G., Lécolier, E., Rivereau, A., Zanni, H., 2004. Chemical structure of cement aged  
554 at normal and elevated temperatures and pressures. *Cem. Concr. Res.* 36, 71–78.

- 555 <https://doi.org/10.1016/j.cemconres.2004.09.018>
- 556 Liu, B., Wang, S., Chen, Y., Gong, C., Lu, L., 2016. Effect of waste gypsum on the setting  
557 and early mechanical properties of belite-C2.75B1.25A3S cement. *J. Therm. Anal.*  
558 *Calorim.* 125, 75–83. <https://doi.org/10.1007/s10973-016-5265-5>
- 559 Lou, W., Guan, B., Wu, Z., 2011. Dehydration behavior of FGD gypsum by simultaneous TG  
560 and DSC analysis. *J. Therm. Anal. Calorim.* 104, 661–669.  
561 <https://doi.org/10.1007/s10973-010-1100-6>
- 562 Lutterotti, L., Matthies, S., Wenk, H.R., 1999. MAUD (Material Analysis Using Diffraction): a  
563 user friendly java program for Rietveld texture analysis and more, in: Jerzy A. Szpunar  
564 (Ed.), *Proceedings of the Twelfth International Conference on Textures of Materials /*  
565 *ICOTOM-12*. National Research Press, Montreal, p. 1599.
- 566 Madsen, I.C., Scarlett, N.V.Y., Kern, A., 2011. Description and survey of methodologies for  
567 the determination of amorphous content via X-ray powder diffraction. *Zeitschrift für Krist.*  
568 226, 944–955. <https://doi.org/10.1524/zkri.2011.1437>
- 569 Matschei, T., Lothenbach, B., Glasser, F.P., 2007. The AFm phase in Portland cement. *Cem.*  
570 *Concr. Res.* 37, 118–130. <https://doi.org/10.1016/j.cemconres.2006.10.010>
- 571 Nguyen, H., Adesanya, E., Ohenoja, K., Kriskova, L., Pontikes, Y., Kinnunen, P., Illikainen,  
572 M., 2019a. By-product based ettringite binder - A synergy between ladle slag and  
573 gypsum. *Constr. Build. Mater.* 197, 143–151.  
574 <https://doi.org/10.1016/j.conbuildmat.2018.11.165>
- 575 Nguyen, H., Kinnunen, P., Carvelli, V., Mastali, M., Illikainen, M., 2019b. Strain hardening  
576 polypropylene fiber reinforced composite from hydrated ladle slag and gypsum.  
577 *Compos. Part B Eng.* 158, 328–338. <https://doi.org/10.1016/j.compositesb.2018.09.056>
- 578 Nguyen, H., Staudacher, M., Kinnunen, P., Carvelli, V., Illikainen, M., 2019c. Multi-fiber  
579 reinforced ettringite-based composites from industrial side streams. *J. Clean. Prod.* 211,  
580 1065–1077. <https://doi.org/10.1016/j.jclepro.2018.11.241>
- 581 Pajares, I., De la Torre, A.G., Martinez-Ramirez, S., Puertas, F., Blanco-Varela, M.-T.,  
582 Aranda, M.A.G., 2002. Quantitative analysis of mineralized white Portland clinkers: The  
583 structure of Fluorellestadite. *Powder Diffr.* 17, 281–286.  
584 <https://doi.org/10.1154/1.1505045>
- 585 Park, J.Y., Byun, H.J., Choi, W.H., Kang, W.H., 2008. Cement paste column for  
586 simultaneous removal of fluoride, phosphate, and nitrate in acidic wastewater.  
587 *Chemosphere* 70, 1429–1437. <https://doi.org/10.1016/j.chemosphere.2007.09.012>
- 588 Pelletier-Chaignat, L., Winnefeld, F., Lothenbach, B., Le Saout, G., Müller, C.J., Famy, C.,  
589 2011. Influence of the calcium sulphate source on the hydration mechanism of Portland  
590 cement – calcium sulphoaluminate clinker – calcium sulphate binders. *Cem. Concr.*  
591 *Compos.* 33, 551–561. <https://doi.org/10.1016/j.cemconcomp.2011.03.005>
- 592 Peysson, S., Péra, J., Chabannet, M., 2005. Immobilization of heavy metals by calcium  
593 sulfoaluminate cement. *Cem. Concr. Res.* 35, 2261–2270.  
594 <https://doi.org/10.1016/j.cemconres.2005.03.015>
- 595 Potgieter, J.H., Potgieter, S.S., Mccrindle, R.I., Strydom, C.A., 2003. An investigation into the  
596 effect of various chemical and physical treatments of a South African phosphogypsum  
597 to render it suitable as a set retarder for cement. *Cem. Concr. Res.* 33, 1223–1227.  
598 [https://doi.org/10.1016/S0008-8846\(03\)00036-X](https://doi.org/10.1016/S0008-8846(03)00036-X)
- 599 Qoku, E., Bier, T.A., Westphal, T., 2017. Phase assemblage in ettringite-forming cement  
600 pastes: A X-ray diffraction and thermal analysis characterization. *J. Build. Eng.* 12, 37–  
601 50. <https://doi.org/10.1016/j.jobte.2017.05.005>



- 602 Quillin, K., 2001. Performance of belite-sulfoaluminate cements. *Cem. Concr. Res.* 31, 1341–  
603 1349. [https://doi.org/10.1016/S0008-8846\(01\)00543-9](https://doi.org/10.1016/S0008-8846(01)00543-9)
- 604 Rashad, A.M., 2017. Phosphogypsum as a construction material. *J. Clean. Prod.* 166, 732–  
605 743. <https://doi.org/10.1016/j.jclepro.2017.08.049>
- 606 Rietveld, H.M., 1969. A profile refinement method for nuclear and magnetic structures. *J.*  
607 *Appl. Crystallogr.* 2, 65–71. <https://doi.org/10.1107/S0021889869006558>
- 608 Roussel, N., Lemaître, A., Flatt, R.J., Coussot, P., 2010. Steady state flow of cement  
609 suspensions: A micromechanical state of the art. *Cem. Concr. Res.* 40, 77–84.  
610 <https://doi.org/10.1016/j.cemconres.2009.08.026>
- 611 Saadaoui, E., Ghazel, N., Ben Romdhane, C., Massoudi, N., 2017. Phosphogypsum:  
612 potential uses and problems – a review. *Int. J. Environ. Stud.* 74, 558–567.  
613 <https://doi.org/10.1080/00207233.2017.1330582>
- 614 Scholtzová, E., Kucková, L., Kožíšek, J., Tunega, D., 2015. Structural and spectroscopic  
615 characterization of ettringite mineral -combined DFT and experimental study. *J. Mol.*  
616 *Struct.* 1100, 215–224. <https://doi.org/10.1016/j.molstruc.2015.06.075>
- 617 Shakhashiro, A., Sansone, U., Wershofen, H., Bollhöfer, A., Kim, C.K., Kim, C.S., Kis-  
618 Benedek, G., Korun, M., Moune, M., Lee, S.H., Tarjan, S., Al-Masri, M.S., 2011. The  
619 new IAEA reference material: IAEA-434 technologically enhanced naturally occurring  
620 radioactive materials (TENORM) in phosphogypsum. *Appl. Radiat. Isot.* 69, 231–236.  
621 <https://doi.org/10.1016/j.apradiso.2010.09.002>
- 622 Shen, Y., Qian, J., Chai, J., Fan, Y., 2014. Calcium sulphoaluminate cements made with  
623 phosphogypsum: Production issues and material properties. *Cem. Concr. Compos.* 48,  
624 67–74. <https://doi.org/10.1016/j.cemconcomp.2014.01.009>
- 625 Silveira, B.I., Dantas, A.E.M., Blasques, J.E.M., Santos, R.K.P., 2003. Effectiveness of  
626 cement-based systems for stabilization and solidification of spent pot liner inorganic  
627 fraction. *J. Hazard. Mater.* 98, 183–190. [https://doi.org/10.1016/S0304-3894\(02\)00317-5](https://doi.org/10.1016/S0304-3894(02)00317-5)
- 628 Smadi, M.M., Haddad, R.H., Akour, A.M., 1999. Potential use of phosphogypsum in  
629 concrete. *Cem. Concr. Res.* 29, 1419–1425. [https://doi.org/10.1016/S0008-8846\(99\)00107-6](https://doi.org/10.1016/S0008-8846(99)00107-6)
- 631 Tayibi, H., Choura, M., López, F.A., Alguacil, F.J., López-Delgado, A., 2009. Environmental  
632 impact and management of phosphogypsum. *J. Environ. Manage.* 90, 2377–2386.  
633 <https://doi.org/10.1016/j.jenvman.2009.03.007>
- 634 Trauchessec, R., Mechling, J.-M., Lecomte, A., Roux, A., Le Rolland, B., 2015. Hydration of  
635 ordinary Portland cement and calcium sulfoaluminate cement blends. *Cem. Concr.*  
636 *Compos.* 56, 106–114. <https://doi.org/10.1016/j.cemconcomp.2014.11.005>
- 637 Wallevik, J.E., 2009. Rheological properties of cement paste: Thixotropic behavior and  
638 structural breakdown. *Cem. Concr. Res.* 39, 14–29.  
639 <https://doi.org/10.1016/j.cemconres.2008.10.001>
- 640 Winnefeld, F., Lothenbach, B., 2010. Hydration of calcium sulfoaluminate cements -  
641 Experimental findings and thermodynamic modelling. *Cem. Concr. Res.* 40, 1239–1247.  
642 <https://doi.org/10.1016/j.cemconres.2009.08.014>
- 643 Yu, Q.L., Brouwers, H.J.H., 2012. Thermal properties and microstructure of gypsum board  
644 and its dehydration products: A theoretical and experimental investigation. *Fire Mater.*  
645 36, 575–589. <https://doi.org/10.1002/fam.1117>
- 646

**1 FEASIBILITY OF INCORPORATING PHOSPHOGYPSUM IN****2 ETTRINGITE-BASED BINDER FROM LADLE SLAG****3 Highlights**

- 4 • Various sources of phosphogypsum were incorporated in an ettringite-based binder.
- 5 • The impurities in phosphogypsum delayed the setting of the developed binders.
- 6 • Polish phosphogypsum led to an increase of 60% in compressive strength.
- 7 • Ettringite-based binders can be produced entirely from industrial side-streams.